Electronic Supporting Information

$NiSe_2$ Anchored N, S-Doped Graphene/Ni Foam as Free-Standing Bi-Functional Electrocatalyst for Efficient Water Splitting

Jinhao Zhou,[1] Zegao Wang,[2,3]* Dongxu Yang[1]*, Fei Qi[1], Xin Hao[4], Wanli Zhang[1], and Yuanfu Chen[1,5]*

[1]School of Electronic Science and Engineering, and State Key Laboratory of Electronic Thin Films and Integrated Devices, University of Electronic Science and Technology of China, Chengdu 610054, P.R China

[2]College of Materials Science and Engineering, Sichuan University, Chengdu 610065, P. R. China

[3]Interdisciplinary Nanoscience Center (iNANO), Aarhus University, Aarhus 8000, Denmark

[4]North Laser Research Institute Co. Ltd., Chengdu, China

[5]Department of Physics, School of Science, and Everest Research Institute, Tibet University, Lhasa 850000, PR China

*Corresponding authors,

Emails: wangzegao@gmail.com, Dongxu_Y@hotmail.com, yfchen@uestc.edu.cn.

Tel: +86-28-83202710.

Materials synthesis

Preparation of 3DSNG/NF and 3DG/NF

The preparation method for 3DSNG and 3DG is from our previous work with a modification[1-4]. In detail, the nickel foams (380 g m^{-2}, 5×10 cm) were washed with diluted HCl, deionized water, isopropanol before they were loaded in a furnace. 200 mg phenothiazine ($C_{12}H_9NS$) was placed upstream of the furnace. The furnace was pumped to 1×10^{-2} Pa before introduction of 300 sccm H_2 and Ar mixed gas. The nickel foams were then heated to 1000 °C and annealed for 20 minutes. After cooling down to 850 °C, the phenothiazine was slowly heated to 180 °C with a heating belt which was slowly sublimed into the furnace. After 30 minutes of growth, the furnace was rapidly cooled to room temperature. The 3DSNG grown on nickel foam can be obtained. For comparison, 3DG was grown on nickel foam using methane as a carbon source at a growth temperature of 1000 °C, and other growth parameters were the same as 3DSNG.

Preparation of $NiSe_2$/3DSNG/NF and $NiSe_2$/3DG/NF

$NiSe_2$/3DSNG/NF was prepared by hydrothermal method. Specifically, 0.632 g of selenium powder (Se) were placed in 65 mL of deionized water. 0.378 g of sodium borohydride ($NaBH_4$) was added drop by drop and stirred for 1 hour. The 3DSNG/NF with the size of 1 cm × 1.5 cm was immersed in the above solution, and slowly stirred to fully infiltrate. it was then transferred to an autoclave and was heated to 180 °C for 10, 15 and 20 hours, respectively. The mass of the $NiSe_2$ could be calculated by weighing the mass of 3DSNG/NF before and after hydrothermal reaction. Unless specific statement, the $NiSe_2$/3DSNG/NF discussed in this study has prepared by a hydrothermal time of 20 hours and the mass of $NiSe_2$ loading is about

2.65 mg. For comparison, we also prepared a $NiSe_2$ and intrinsic graphene foam composite ($NiSe_2$/3DG/NF) with the same synthesis parameters.

Materials Characterizations

Scanning electron microscope (SEM) was performed on a JEOL JSM-7000F. Transmission electron microscope (TEM) images were obtained by using a Tecnai F20 at 200 kV. Elemental distribution was studied using energy dispersive X-ray spectroscopy on a Tecnai F20 equipped with an Oxford/INCA EDS. The X-ray diffraction (XRD) patterns were obtained by a X'Pert PRO (PNAlytical) with a Cu Kα irradiation (λ = 1.54 Å). X-ray photoelectron spectroscopy (XPS) results were recorded by a Kratos XSAM800 with Al Ka radiation (144 W, 12 mA, 12 kV). Raman spectra were recorded by using a Renishaw Raman spectrometer with a 532 nm laser.

Electrochemical measurements

$NiSe_2$/3DG/NF, $NiSe_2$/3DG/NF, 3DSNG/NF, 3DG/NF, NF can be directedly used as electrode with the contact area in the electrolyte of 1.0 cm^2. The commercial 20% Pt/C catalyst was prepared with 20 mg Pt/C in 1 mL water/ethanol (1:1 by volume), and then 60 μL of Nafion solution was added and sonicated for 30 minutes. Then, it was loaded on nickel foam with a pipette. The mass loading of Pt/C is about 2.70 mg cm^{-2}. The counter electrode was carbon rod and reference electrode was saturated calomel (SCE) (in acid electrolyte) and Hg/HgO (in alkaline electrolyte), respectively. The SCE potential $E_{(SCE)}$ and Hg/HgO potential $E_{(Hg/HgO)}$ was converted to a reversible hydrogen electrode potential $E_{(RHE)}$ by $E_{(RHE)} = E(SCE) + 0.245$ V + 0.059 pH and $E_{(RHE)} = E_{(Hg/HgO)} + 0.098$ V + 0.059 pH. The polarization curves were recorded by linear sweep voltammetry at a scan rate of 0.5 mV s^{-1} with iR compensation. The oxygen evolution overpotential (η) is calculated by $\eta = E_{(RHE)}$ - 1.23 V. The amount of H_2 and O_2 was detected with an on-line gas chromatography (GC9790, using argon as a carrier gas) at constant current of 10, 30 and 50 mA in case of water splitting every 5 min. The Faradaic efficiency is calculated as the ratio of measured amount of H_2 and O_2 and theoretical amount of H_2 and O_2 according to Faraday's law.

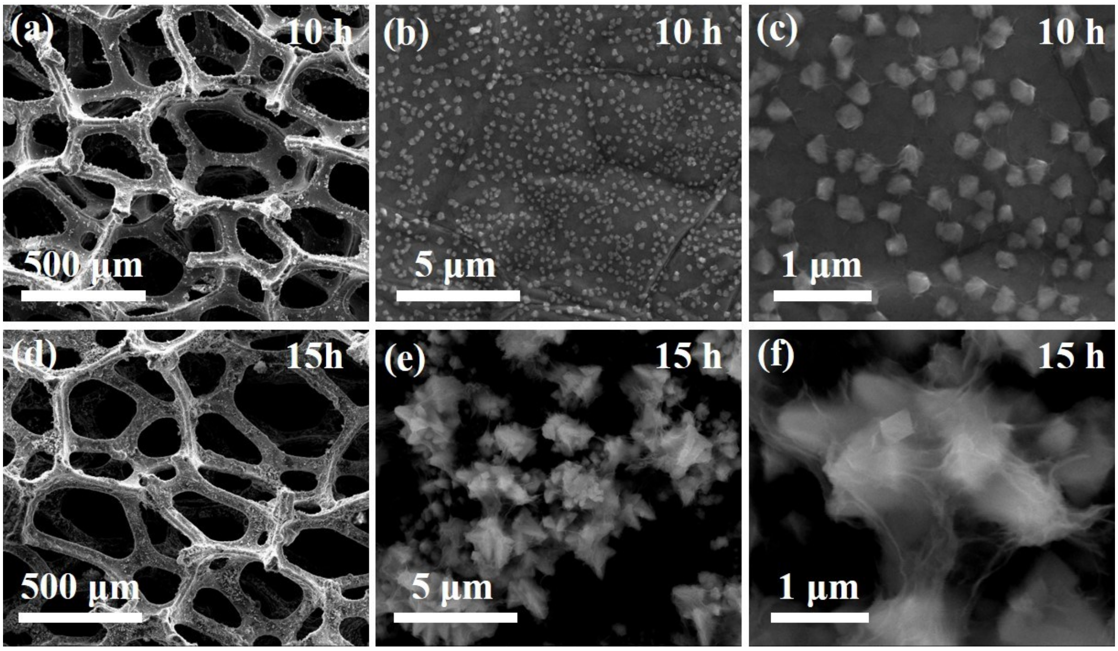

Figure S1. SEM images of $NiSe_2$/3DSNG/NF. (a-c) hydrothermal reaction time is 10 hours; (d-f) hydrothermal reaction time is 15 hours.

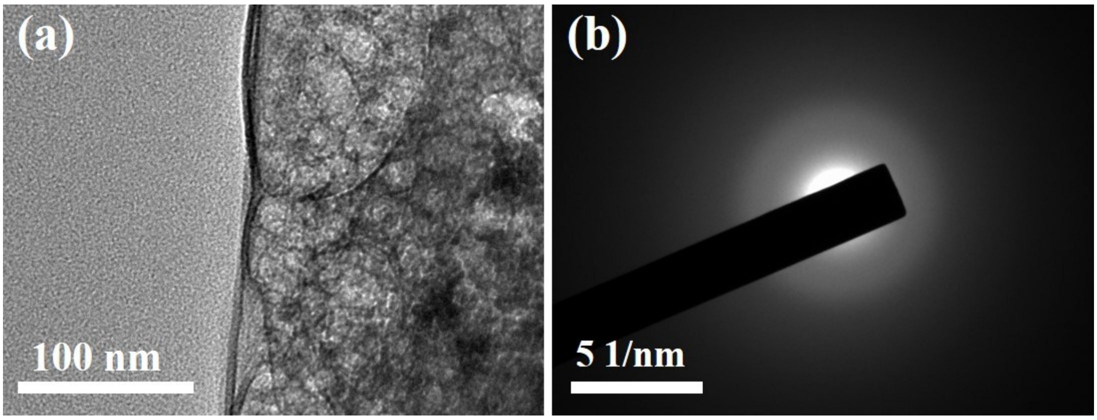

Figure S2. The TEM image (a) and corresponding SAED pattern (b) of 3DSNG.

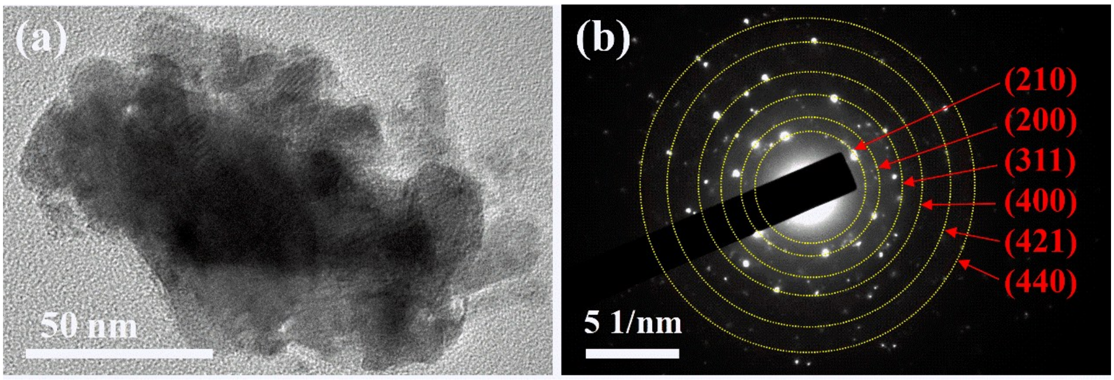

Figure S3. The TEM image (a) and corresponding SAED pattern (b) of $NiSe_2$/3DSNG.

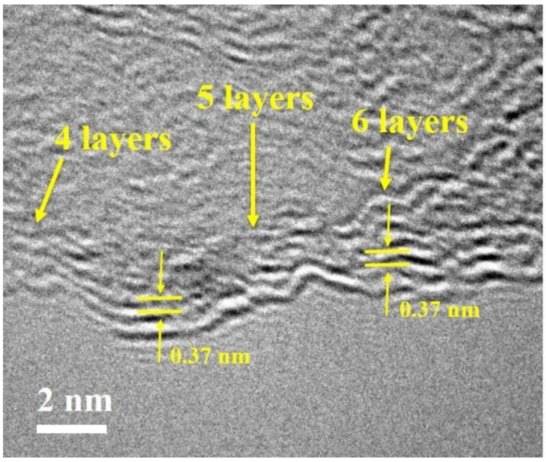

Figure S4. HRTEM image of 3DSNG exfoliated from 3DSNG/NF.

Table S1. The ICP-MS results of N and S doping contents in 3DSNG/NF. Sample A and B are 3DSNG/NF before and after hydrothermal reaction, respectively.

Samples	Element	Content (at%)
A	N	2.57
A	S	2.96
B	N	2.55
B	S	2.95

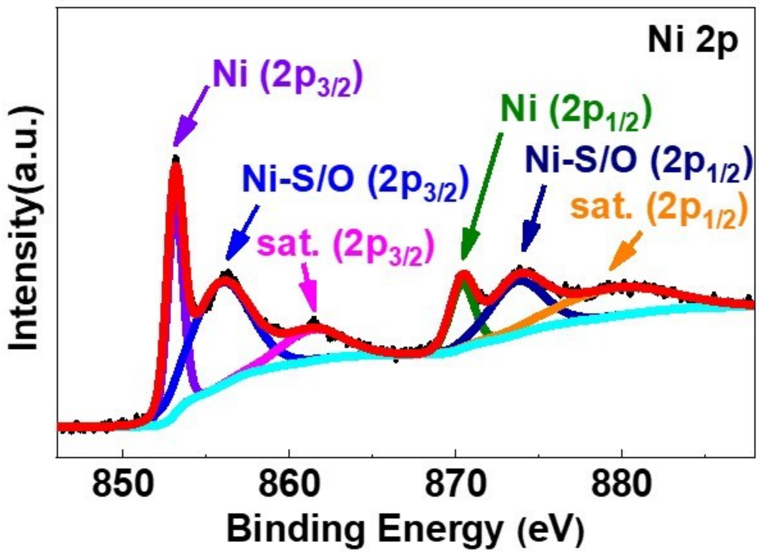

Figure S5. The Ni spectrum of 3DSNG/NF before loading of $NiSe_2$.

Table S2 Comparison of HER catalytic performance of $NiSe_2$/3DSNG/NF and the reference group in 0.5 M H_2SO_4.

Samples	η_{10} (mV)	η_{50} (mV)	η_{100} (mV)	Tafel slop (mV dec^{-1})
$NiSe_2$/3DSNG/NF	130	192	221	28.56
$NiSe_2$/3DG/NF	205	277	315	43.46
3DSNG/NF	223	316	366	48.62
3DG/NF	283	379	430	98.74
NF	382	488	528	183.91
Pt/C	45	74	94	32.55

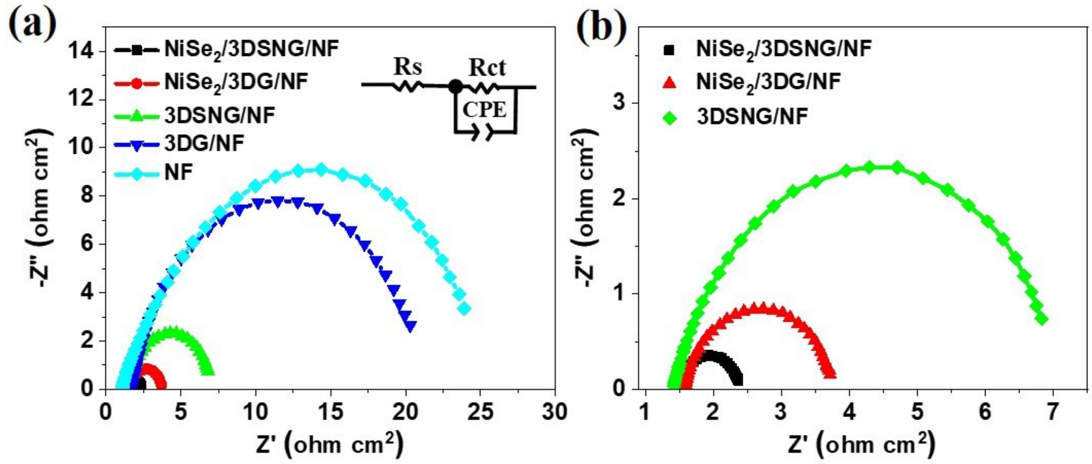

Figure S6. (a) Nyquist diagram of $NiSe_2$/3DSNG/NF and the reference group at 300 mV overpotential; (b) Nyquist plot after amplification.

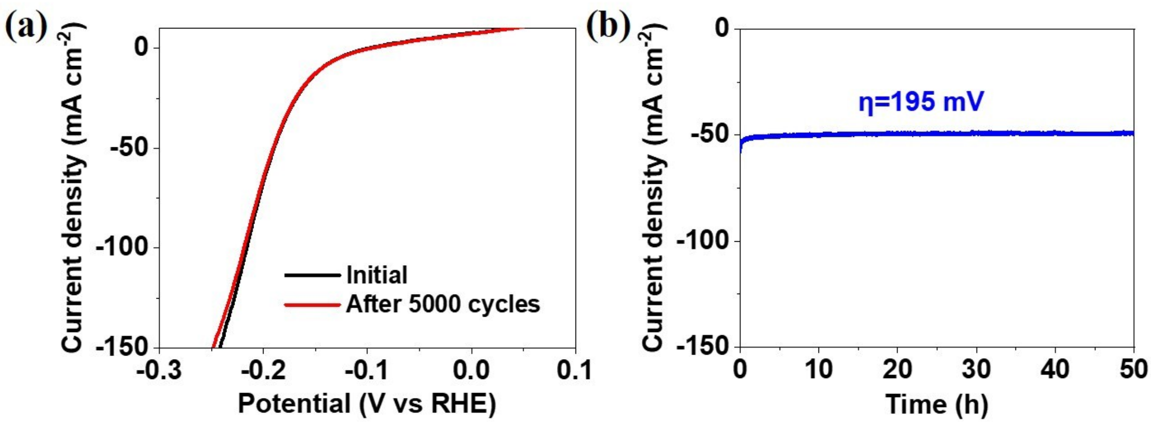

Figure S7. (a) polarization curve of $NiSe_2$/3DSNG/NF in 0.5 M H_2SO_4 before and after 5000 cycles; (b) current-time curve at overpotential of 195 mV.

Table S3 Comparison of HER catalytic performance of $NiSe_2$/3DSNG/NF and the reference group in 1 M KOH.

Samples	η_{10} (mV)	η_{50} (mV)	η_{100} (mV)	Tafel slop (mV dec^{-1})
$NiSe_2$/3DSNG/NF	177	247	269	75.95
3DSNG/NF	226	299	331	103.31
NF	265	395	493	165.94
Pt/C	64	84	101	42.77

Table S4. Comparison of HER performance of $NiSe_2$/3DSNG/NF with other reported highly active HER electrocatalysts.

Catalysts	Overpotential@j ($mV@mA\ cm^{-2}$)	Electrolytes	Ref.
$NiSe_2$/3DSNG/NF	269@100	1 M KOH	This work
$NiSe_2$/3DSNG/NF	247@50	1 M KOH	This work
$NiSe_2$/3DSNG/NF	177@10	1 M KOH	This work
$NiSe_2$-Ni_2P/NF	102@10	1 M KOH	5
CoP/NCNHP	115@10	1M KOH	6
NiCoP	124@10	1M KOH	7
CoSe/Ti	121@10	1M KOH	8
NiSn@C	160@10	1M NaOH	9
WP/CC	150@10	1M KOH	10
Co-Ni-B	133@10	1M NaOH	11
Co-Mo-S_x	~201@5	0.1M KOH	12

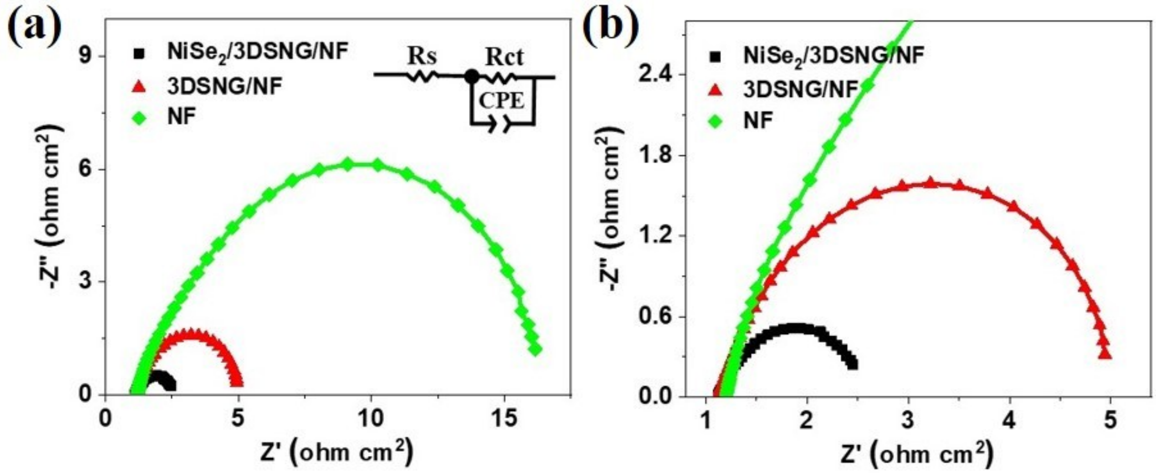

Figure S8. (a) Nyquist diagram of $NiSe_2$/3DSNG/NF and the reference group at 300 mV overpotential in 1 M KOH; (b) Nyquist plot after amplification.

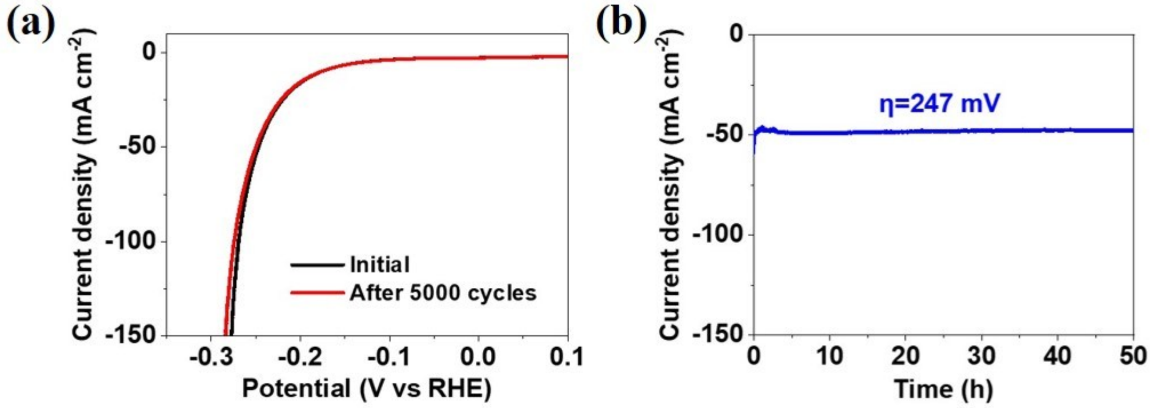

Figure S9. (a) polarization curve of $NiSe_2$/3DSNG/NF in 1 M KOH before and after 5000 cycles; (b) current-time curve at overpotential of 247 mV.

Table S5 Comparison of OER catalytic performance of $NiSe_2$/3DSNG/NF and the control group in 1 M KOH.

Samples	η_{10} (mV)	η_{50} (mV)	η_{100} (mV)	Tafel slop (mV dec^{-1})
$NiSe_2$/3DSNG/NF	94 (Ni^{2+} oxidation)	124 (Ni^{2+} oxidation)	256	42.89
3DSNG/NF	296	329	348	47.16
NF	428	613	760	174.44
RuO_2	280	378	418	79.83

Table S6. Comparison of OER performance of $NiSe_2$/3DSNG/NF with other reported highly active OER electrocatalysts.

Catalysts	Overpotential@j (mV @ mA cm^{-2})	Electrolytes	Ref.
$NiSe_2$/3DSNG/NF	256@100	1 M KOH	This work
$NiSe_2$/3DSNG/NF	124@50 (Ni^{2+} oxidation)	1 M KOH	This work
$NiSe_2$/3DSNG/NF	94@10 (Ni^{2+} oxidation)	1 M KOH	This work
$NiSe_2$-Ni_2P/NF	183@10	1 M KOH	5
Co_4N/CC	257@10	1 M KOH	13
NiFe LDHs	305@10	1 M KOH	14
$Ni_{45}Fe_{55}$ oxyhydroxide	310@10	0.1 M KOH	15
CoCr LDH	340@10	1 M NaOH	16
Ni-Co-P HNBs	270@10	1 M KOH	17
Ni_3N/NF	399@20	1 M KOH	18
$Na_{0.08}Ni_{0.9}Fe_{0.1}O_2$	260@10	1 M KOH	19

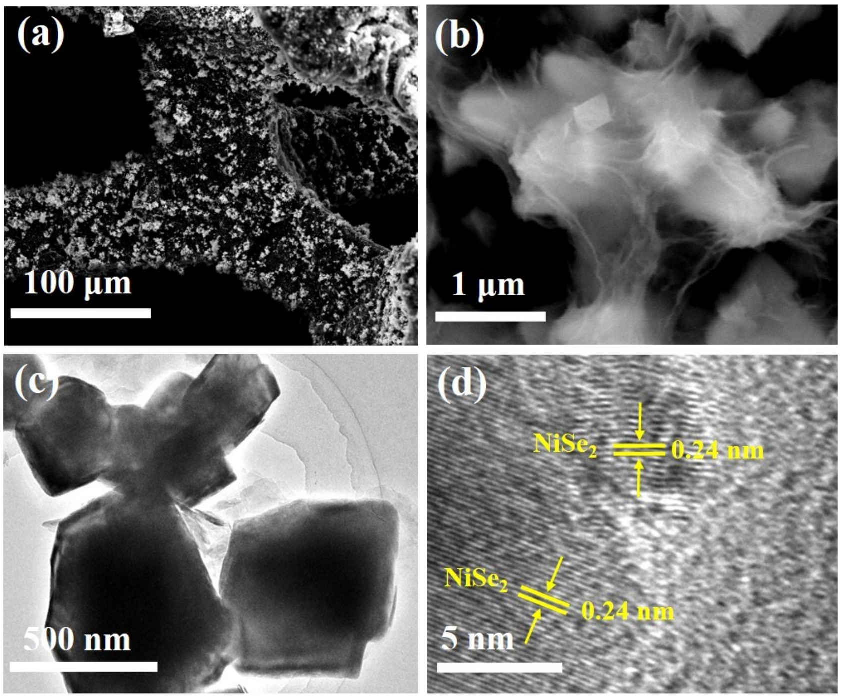

Figure S10. The SEM (a and b) and TEM (c and d) images of the $NiSe_2$/3DSNG/NF after the stability test.

Table S7. Comparison of overall water splitting performance for the electrolyzer assembled by two $NiSe_2$/3DSNG/NF electrodes with other reported alkaline electrolyzer assembled by bifunctional catalysts.

Catalysts	Voltage (V) @10 mA cm^{-2}	Electrolytes	Ref.
$NiSe_2$/3DSNG/NF	1.59	1 M KOH	This work
NiFeRu-LDH	1.52	1 M KOH	20
$Ni_{0.51}Co_{0.49}P$	1.57	1 M KOH	21
NiCoP	1.64	1 M KOH	22
Ni-Fe-P	1.67	1 M KOH	23
MoO_2/NF	1.53	1 M KOH	24
Cu@NiFe LDH	1.54	1 M KOH	25
$FeNi_3N$/NF	1.62	1 M KOH	26
Co_4NiP	1.59	1 M KOH	27
Ni_3Se_2/NF	1.61	1 M KOH	28

References

[1] He, J.; Chen, Y.; Lv, W.; Wen, K.; Li, P.; Qi, F.; Wang, Z.; Zhang, W.; Li, Y.; Qin, W.; He, W. Highly-Flexible 3D Li_2S/graphene Cathode for High-Performance Lithium Sulfur Batteries. *J. Power Sources 327 (***2016)** 474-480.

[2] Qi, F.; Li, P.; Chen, Y.; Zheng, B.; Liu, J.; Zhou, J.; He, J.; Hao, X.; Zhang, W. Three-Dimensional Structure of WS_2/graphene/Ni as a Binder-Free Electrocatalytic Electrode for Highly Effective and Stable Hydrogen Evolution Reaction. *Int. J. Hydrogen Energ. 42 (***2017)** 7811-7819.

[3] Zhou, J.; Wang, Z.; Chen, Y.; Liu, J.; Zheng, B.; Zhang, W.; Li, Y. Growth and Properties of Large-Area Sulfur-Doped Graphene Films. *J. Mater. Chem. C. 5 (***2017)** 7944-7949.

[4] Zhou, J.; Yue, H.; Qi, F.; Wang, H.; Chen, Y. Significantly Enhanced Electrocatalytic Properties of Three-Dimensional Graphene Foam Via Ar Plasma Pretreatment and N, S Co-Doping. *Int. J. Hydrogen Energ. 42 (***2017)** 27004-27012.

[5] Wang, S., He, P., Jia, L., He, M., Zhang, T., Dong, F., Liu, M., Liu, H., Zhang, Y., Li, C., Gao, J. and Bian, L., *Applied Catalysis B: Environmental*, 243 (**2019**) 463-469.

[6] Y. Pan, K. Sun, S. Liu, X. Cao, K. Wu, W.C. Cheong, Z. Chen, Y. Wang, Y. Li, Y. Liu, D. Wang, Q. Peng, C. Chen, Y. Li, Core-shell ZIF-8@ZIF-67-derived CoP nanoparticle-embedded N-doped carbon nanotube hollow polyhedron for efficient overall water splitting, J. Am. Chem. Soc. 140 (**2018**) 2610-2618.

[7] Y. Li, J. Liu, C. Chen, X. Zhang, J. Chen, Preparation of NiCoP hollow quasi-polyhedra and their electrocatalytic properties for hydrogen evolution in alkaline solution, ACS Appl. Mater. Interfaces 9 (**2017**) 5982-5991.

[8] T. Liu, Q. Liu, A.M. Asiri, Y. Luo, X. Sun, An amorphous CoSe film behaves as an active and stable full water-splitting electrocatalyst under strongly alkaline conditions, Chem. Commun. 51 (**2015**) 16683-16686.

[9] L. Lang, Y. Shi, J. Wang, F.B. Wang, X.H. Xia, Hollow core-shell structured Ni-Sn@C nanoparticles: a novel electrocatalyst for the hydrogen evolution reaction, ACS Appl. Mater. Interfaces 7 (**2015**) 9098-9102.

[10] Z. Pu, Q. Liu, A.M. Asiri, X. Sun, Tungsten phosphide nanorod arrays directly grown on carbon cloth: a highly efficient and stable hydrogen evolution cathode at all pH values, ACS Appl. Mater. Interfaces 6 (**2014**) 21874-21879.

[11] S. Gupta, N. Patel, R. Fernandes, R. Kadrekar, A. Dashora, A.K. Yadav, D. Bhattacharyya, S.N. Jha, A. Miotello, D.C. Kothari, Co–Ni–B nanocatalyst for efficient hydrogen evolution reaction in wide pH range, Appl. Catal., B 192 (**2016**) 126-133.

[12] J. S. Jirkovsky, C. D. Malliakas, P. P. Lopes, N. Danilovic, S. S. Kota, K. C. Chang, B. Genorio, D. Strmcnik, V. R. Stamenkovic, M. G. Kanatzidis, N. M. Markovic, Design of active and stable Co–Mo–S_x chalcogels as pH-universal catalysts for the hydrogen evolution reaction. Nat. Mater. 15 (**2016**) 197-203.

[13] P. Chen, K. Xu, Z. Fang, Y. Tong, J. Wu, X. Lu, X. Peng, H. Ding, C. Wu, Y. Xie, Metallic Co_4N porous nanowire arrays activated by surface oxidation as electrocatalysts for the oxygen evolution reaction, Angew. Chem. Int. Ed. 54 (**2015**) 14710-14714.

[14] F. Song, X. Hu, Exfoliation of layered double hydroxides for enhanced oxygen evolution catalysis, Nat. Commun. 5 (**2014**) 4477.

[15] M. Görlin, P. Chernev, J. Ferreira de Araújo, T. Reier, S. Dresp, B. Paul, R. Krähnert, H. Dau, P. Strasser, Oxygen evolution reaction dynamics, faradaic charge efficiency, and the active metal redox states of Ni–Fe oxide water splitting electrocatalysts, J. Am. Chem. Soc. 138 (**2016**) 5603-5614.

[16] C. Dong, X. Yuan, X. Wang, X. Liu, W. Dong, R. Wang, Y. Duan, F. Huang, Rational design of cobalt–chromium layered double hydroxide as a highly efficient electrocatalyst for water oxidation, J. Mater. Chem. A 4 (**2016**) 11292-11298.

[17] E. Hu, Y. Feng, J. Nai, D. Zhao, Y. Hu, X.W. Lou, Construction of hierarchical Ni–Co–P hollow nanobricks with oriented nanosheets for efficient overall water splitting, Energy Environ. Sci. 11 (**2018**) 872-880.

[18] M. Shalom, D. Ressnig, X. Yang, G. Clavel, T.P. Fellinger, M. Antonietti, Nickel nitride as an efficient electrocatalyst for water splitting, J. Mater. Chem. A 3 (**2015**) 8171-8177.

[19] B. Weng, F. Xu, C. Wang, W. Meng, C.R. Grice, Y. Yan, A layered $Na_{1-x}Ni_yFe_{1-y}O_2$ double oxide oxygen evolution reaction electrocatalyst for highly efficient water-splitting, Energy Environ. Sci. 10 (**2017**) 121-128.

[20] G. Chen, T. Wang, J. Zhang, P. Liu, H. Sun, X. Zhuang, M. Chen, X. Feng, Accelerated hydrogen evolution kinetics on NiFe-layered double hydroxide electrocatalysts by tailoring water dissociation active sites, Adv. Mater. 30 (**2018**) 1706279.

[21] J. Yu, Q. Li, Y. Li, C.-Y. Xu, L. Zhen, V.P. Dravid, J. Wu, Ternary metal phosphide with triple-Layered structure as a low-cost and efficient electrocatalyst for bifunctional water splitting, Adv. Funct. Mater. 26 (**2016**) 7644-7651.

[22] J. Li, G. Wei, Y. Zhu, Y. Xi, X. Pan, Y. Ji, I.V. Zatovsky, W. Han, Hierarchical NiCoP nanocone arrays supported on Ni foam as an efficient and stable bifunctional electrocatalyst for overall water splitting, J. Mater. Chem. A 5 (**2017**) 14828-14837.

[23] C. Xuan, J. Wang, W. Xia, Z. Peng, Z. Wu, W. Lei, K. Xia, H.L. Xin, D. Wang, Porous structured Ni-Fe-P nanocubes derived from a prussian blue analogue as an electrocatalyst for efficient overall water splitting, ACS Appl. Mater. Interfaces 9 (**2017**) 26134-26142.

[24] Y. Jin, H. Wang, J. Li, X. Yue, Y. Han, P.K. Shen, Y. Cui, Porous MoO_2 nanosheets as non-noble bifunctional electrocatalysts for overall water splitting, Adv. Mater. 28 (**2016**) 3785-3790.

[25] L. Yu, H. Zhou, J. Sun, F. Qin, F. Yu, J. Bao, Y. Yu, S. Chen, Z. Ren, Cu nanowires shelled with NiFe layered double hydroxide nanosheets as bifunctional electrocatalysts for overall water splitting, Energy Environ. Sci. 10 (**2017**) 1820-1827.

[26] B. Zhang, C. Xiao, S. Xie, J. Liang, X. Chen, Y. Tang, Iron–nickel nitride nanostructures in situ grown on surface-redox-etching nickel foam: efficient and ultrasustainable electrocatalysts for overall water splitting, Chem. Mater. 28 (**2016**) 6934-6941.

[27] L. Yan, L. Cao, P. Dai, X. Gu, D. Liu, L. Li, Y. Wang, X. Zhao, Metal-organic frameworks derived nanotube of nickel-cobalt bimetal phosphides as highly efficient electrocatalysts for overall water splitting, Adv. Funct. Mater. 27 (**2017**) 1703455.

[28] R. Xu, R. Wu, Y. Shi, J. Zhang, B. Zhang, Ni_3Se_2 nanoforest/Ni foam as a hydrophilic, metallic, and self-supported bifunctional electrocatalyst for both H_2 and O_2 generations, Nano Energy 24 (**2016**) 103-110.